RESEARCH PAPER

Revolutionizing cancer therapies: tin-doped zinc sulfide nanoparticles for oxidative stress mitigation and safe applications in mice models

Tariq Aziz[1], Fazal Akbar Jan[2], Naimat Ullah[3], Haleema Sadia[1], Hussain Ahmad[4]*

[1]*Animal and Human Physiology Laboratory, Department of Zoology, Quaid-i-Azam University, Islamabad, Pakistan*
[2]*Department of Chemistry, Bacha Khan University, Charsadda, Khyber-Pakhtunkhwa, Pakistan*
[3]*Department of Chemistry, Quaid-i-Azam University, Islamabad, Pakistan*
[4]*Department of Zoology, University of Malakand, Chakdarra, Dir Lower, Pakistan*

ABSTRACT

Objective(s): Nanotechnology is a rapidly growing field with broad applications across medicine, biology, chemistry, and engineering, largely due to nanoparticles' unique physical and chemical properties. In cancer treatment, nanoparticles offer significant potential for both diagnosis and therapy. This study synthesized tin-doped zinc sulfide nanoparticles (Sn-doped ZnS NPs) and undoped zinc sulfide nanoparticles (ZnS NPs) to explore their therapeutic effects on the brain, kidney, and liver of mice.

Materials and Methods: The nanoparticles were synthesized using a wet chemical method and characterized by X-ray diffraction (XRD), scanning electron microscopy (SEM), Fourier-transform infrared (FTIR) spectroscopy, UV-Vis spectroscopy, and energy-dispersive X-ray spectroscopy (EDX). Biological evaluations were performed by administering ZnS and Sn-doped ZnS NPs to BALB/c mice. These assessments included measurements of organ weights, oxidative stress biomarkers such as thiobarbituric acid reactive substances (TBARS) and reactive oxygen species (ROS), antioxidant enzyme activities such as catalase (CAT), peroxidase (POD), superoxide dismutase (SOD), reduced glutathione (GSH), and histopathological analysis of key organs.

Results and Conclusions: Sn-doped ZnS NPs demonstrated enhanced structural and optical properties, along with significant antioxidant effects, without causing notable toxicity in vital organs. These findings suggest that Sn-doped ZnS NPs have strong potential for therapeutic applications, particularly in cancer treatment, and warrant further investigation to elucidate their mechanistic roles and long-term safety.

Keywords: *Cancer; Zinc Sulfide Nanoparticles; Oxidative stress; Nanoparticles based therapy; Antioxidant Enzymes*

How to cite this article

Aziz T, Jan F.A, Ullah N, Sadia H, Ahmad H. Revolutionizing cancer therapies: tin-doped zinc sulfide nanoparticles for oxidative stress mitigation and safe applications in mice models. Nanomed J. 2026; 13: 1-. DOI: 10.22038/NMJ.2025.86892.2196

INTRODUCTION

The advancement of nanotechnology, particularly nanoparticles, offers an innovative and enabling platform that promises a wide range of novel uses in medicine, biology, chemistry, and engineering. These applications have great potential for precise diagnosis, early disease detection, and cancer treatment [1]. An intriguing advance in current nanotechnology research is the biological synthesis of semiconductor nanoparticles. Today, there is significant excitement in the literature regarding the multidisciplinary field of nanobiotechnology and its applications in biological systems [2, 3].

A common and crucial trace element in biological systems is zinc (Zn). The Zn ion regulates cell proliferation, differentiation, and both apoptotic and necrotic cell death by acting as a structural component in many proteins and transcription factors and as a catalytic component of several enzymes [4]. The liver significantly influences Zn homeostasis, which controls how Zn ions are combined into a wide range of enzymes essential to the body's metabolism [5]. Zn is vital for triggering the manufacture of protein in the liver and kidneys [6]. Zinc is generally involved in a variety of processes that keep the cell's redox equilibrium stable. These include: (i) managing the production of oxidants and the oxidative damage that metals cause; (ii) the dynamic interaction of zinc with sulfur in protein cysteine cluster cause to liberate the metal from oxidized glutathione, peroxides, nitric oxide, and other thiol oxidant species; (iii) zinc's function in controlling glutathione metabolism and the general thiol redox status of proteins; (iv) either direct or indirect

**Corresponding author(s):* Fazal Akbar Jan, Department of Chemistry, Bacha Khan University, Charsadda, Khyber-Pakhtunkhwa, Pakistan. Email: *fazal_akbarchem@yahoo.com.*

Note. This manuscript was submitted on March 19, 2025; approved on October 01, 2025.

regulation of redox signaling; and (v) stimulation of zinc-binding proteins that release the metal under oxidative stress and act as a scavenging oxidant independently [7]. Sulfur (S) is a mineral necessary for life and found in amino acids [8]. Sulfur has been demonstrated to have metabolic reprogramming and anti-cancer activity [9].

The zinc and sulfide combine to form zinc sulfide (ZnS), which is one of the nanoparticles found in organic-rich sediments, anaerobic soil, wastewater effluent, biosolid sand, and sulfidic environments [10-12]. ZnS NPs are interesting because they are superior II-VI semiconductors with a wide band gap energy of 3.7 eV at 300 K. [13]. ZnS is widely used in optoelectronics and biomedicine, including laser technology, photocatalysis, nanogenerators, biosensors [14], bio-applications as protein sensors, imaging, and antimicrobial agents [15, 16]. Zinc sulfide nanoparticles (ZnS NPs) have also demonstrated potent cytotoxic effects against human acute myeloid leukemia (KG-1A) cells, inducing apoptosis through the generation of ROS and the secretion of TNF-α, while showing no toxicity to normal lymphocytes. These findings suggest the potential of ZnS NPs for targeted cancer treatment [17]. An imbalance between oxidants and antioxidants causes oxidative damage in cells and tissues, and may even lead to cancer due to excessive ROS production and decreased antioxidant levels [18, 19]. Zinc sulfide nanoparticles have demonstrated significant cytotoxic effects against human acute myeloid leukemia (KG-1A) cells in vitro, primarily through the generation of ROS and induction of apoptosis. These findings highlight their potential for targeted cancer therapies. In this study, we investigate the role of both doped and undoped ZnS nanoparticles in modulating antioxidant and oxidant markers in brain, kidney, and liver of mice in vivo. This research will provide insights into how ZnS nanoparticles influence oxidative stress and antioxidant defense mechanisms in these critical organs within a living organism.

MATERIALS AND METHODS

Reagents and supplies

Chemical were obtained from Sigma-Aldrich (Sigma, St. Louis, Missouri, USA) Chloroform, N.N-Diethyl-p-phenyl diamine sulfate (DEPPD), Formaldehyde, Nitro blue tetrazolium (NBT), ferrous sulfate, Coomassie blue, Hematoxylin, Triton-x100, Bovine Serum Albumin (BSA), Sodium Dodecyl Sulfate (SDS), Phenylmethylsulfonyl fluoride (PMSF), potassium phosphate monobasic, Sodium azide, Sodium phosphate dibasic, Sodium chloride, Trichloroacetic acid (TCA), Sodium Hydroxide Hydrogen peroxide, Guaicol, Tri-sodium Citrate, Tris(hydroxymethyl)aminomethane hydrochloride (Tris-HCL), tert-Butyl alcohol (TBA), Potassium chloride, Riboflavin, L-Methionine, Eosin, 5,5'-Dithiobis(2-nitrobenzoic acid) (DTNB), phosphoric acid, Methanol.

Synthesis of doped and undoped ZnS NPs

Zinc sulfide nanoparticles were synthesized using a wet chemical method. In this approach, zinc acetate served as the zinc source, while sodium sulfide was employed as the sulfur source. Zinc acetate was prepared using N, N-dimethylformamide (DMF) as the solvent. The synthesis procedure comprised the following steps: Initially, zinc acetate (0.2 M) solution was dissolved in 15 mL of DMF, and the mixture was agitated for 10 minutes. Sodium sulfide solution was added dropwise to the zinc acetate solution and stirred continuously for 2.5 hours until a greyish-white zinc sulfide precipitate formed. The product was then centrifuged and washed several times with methanol and deionized water. Finally, the obtained material was dried in an oven at 60 °C to yield ZnS nanoparticles. For tin-doped ZnS NPs synthesis, the same method was used except that some weight percentage of $SnCl_4.5H_2O$ was added to the DMF solvent and stirred for half an hour before adding the zinc acetate.

Design experiment and animals

Six-week-old Albino mice (BALB/c) were categorized into three groups. Each group had six male mice. Group I (Control group, n = 6) orally received saline solution. Group II (n = 6) intraperitoneally (i.p) received undoped ZnS (5 mg/kg body weight), and group III (n = 6) i.p received Sn-doped ZnS (5 mg/kg body weight). The doses were used on alternate days up to 14 days. The experiment was approved by the Bioethical Committee of Biological Sciences on the use and care of animals (No.BEC-FBS-QAU2019-156).

Preparation of extract buffer (Lysing buffer)

The lysing buffer was prepared by dissolving 0.5 g SDS, 0.1 g sodium azide, 4.38 g NaCl, and 5.95 g HEPES in 495 mL of distilled water. Triton X-100 (5 mL) was then added to make the final volume 500 mL [20, 21].

Method of preparation of tissue homogenate

A manual homogenizer (GPE Limited, UK) was used to mince the tissues (brain, kidney, and liver, each 100 mg) in frosted Petri dishes. Tissues were

homogenized in 1 mL of extract buffer (pH 7.0), which also contained 0.1mg of PMSF. The homogenate was then centrifuged at 5031 × g for 10 min to separate the supernatant. The resulting supernatant was transferred into labeled 1.5 mL Eppendorf tubes and kept at −20 °C for subsequent biochemical analyses [20].

Determination of oxidative stress biomarkers in organs

Tissue homogenate was kept at -20°C until each sample was analysed for oxidative stress biomarkers.

Lipid Peroxidation assay

To quantify the TBARS level in tissue samples to serve as a biomarker of lipid peroxidation using lipid peroxidation assay according to [22]. The procedure was as follows: 100 microliter (µl) of homogenized samples were combined with 50 mM Tris-HCl, 1.5 mM ascorbic acid, 1 mM FeSO4, and 600 µl of distilled water. Afterward, the mixture was incubated at 37 °C for 15 minutes. To stop the reaction, 1 milliliter (0.37% w/v) of thiobarbituric acid was supplemented. Following the addition of 1 milliliter of 10% trichloroacetic acid to each sample, the reaction mixtures were heated in a water bath to 90 °C for 15 minutes. After cooling, the mixture was centrifuged for 10 minutes at 1000g. After separating the supernatant, the amount of TBARS in each sample was calculated using absorption measurement at 532 nm. To express the results, nanomoles of malonaldehyde per minute per milligram of tissue were used, with 156 mmol/L/cm as the molar extinction coefficient.

Reactive oxygen species (ROS)

The method employed for quantifying the levels of reactive oxygen species (ROS) in each tissue homogenate was utilized [23]. The reagent solution consisted of ferrous sulfate, sodium acetate buffer (0.1 M, pH 4.8), and 10 mg DEPPD in sodium acetate buffer. Next, working reagents (1680 µl) and 0.1 M sodium acetate buffer (1200 µl, pH 4.8) were mixed with tissue homogenate (60 µl) or 30% H_2O_2. At 37 °C, the contents were incubated for 1 minute. The absorbance was determined with a UV-visible spectrophotometer at 505 nm. For every sample, three measurements were made at intervals of 15 seconds. The ROS one unit was equal to one milligram of hydrogen peroxide in the sample.

Antioxidant enzymes

Enzymatic and non-enzymatic antioxidants determination are CAT, SOD, POD and GSH.

Catalase assay (CAT)

The CAT activity determination in tissue homogenate followed the previously published protocol [24]. To follow the procedure, tissue homogenate (0.1 mL), 1 mL H_2O_2 (5.9 mM) and 50 mM potassium phosphate buffer (1.99 mL, pH 7.0) were combined in 3 mL cuvette. The absorbance of each sample was instantly read at 240 nm with intervals of 15 and 30 seconds, and the values were averaged. In the blank sample, the reagent combination was supplemented with distilled water rather than homogenate. Alteration in absorbance of 0.01 U/min was considered to be one unit of CAT activity.

Superoxide dismutase (SOD)

SOD concentration was determined using the procedure outlines by [25]. After making a 10% (w/v) tissue homogenate in phosphate buffer (0.05 M, pH 7.8), the mixture was centrifuged for 15 min at 10,000 RPM. In a test tube, 0.4 mL of NBT (24_M), 1 mL of 50 mM sodium carbonate and 0.2 mL of 0.1 mM EDTA were vortexed with the resultant supernatant (0.5 mL). Next, hydroxylamine hydrochloride (0.4 mL, 1 mM) was added to maintain the reaction. The absorbance of SOD was measured at 560 nm and sample without tissue homogenate take as a negative control.

Peroxidase (POD)

The reaction mixtures and tissue homogenate were prepared according to the protocol described by [24]. That is made by combining 100 µl of tissue homogenate, 100 µl of guaiacol (20 mM), and 2.5 mL of 50 mM phosphate buffer. Then homogenate was mixing and started the reaction by adding 300 µl of H_2O_2 (40 mM). After 1 min, the absorbance of the reaction mixture was read at 470 nm. One unit of POD activity was defined as a 0.01 U/min change in absorbance.

Determination of reduced glutathione (GSH)

GSH concentration was measured by using the method outlines by [26]. The reagent solution contained tissue homogenate, DTNB disodium phosphate buffer (0.4 M) and (5,5-dithiobis (2-nitrobenzoic acid)). 40 milligrams of DTNB were dissolved in 100 mL of one percent tri-sodium citrate to make DTNB. The unit of measurement for GSH activity was mols/g, and the absorption was recorded at 412 nm after a yellow hue appeared.

Estimation of total protein

Total Protein was quantified in the kidney, liver, and brain by using the standard Bradford assay.

Histology and morphometry

Five micrometer-thick tissue sections were stained with Harris' hematoxylin. Sections were washed, stained, dehydrated, and then washed in DPX. Sections were examined at 10x and 40x magnification on a photomicroscope (Olympus Japan). Adobe Photoshop was used to prepare image panels (Version 7.0, Microsoft Inc., USA).

For cellular morphometry, six arbitrary slices from each group's liver, kidney, and brain tissues were employed. Using the Image J program at a 40x magnification (ver.1.8.0, Microsoft Inc. USA), hepatocyte area and hepatocyte nucleus area were evaluated for the liver, glomerular area and renal corpuscular area were calculated for the kidneys, and neuron area was evaluated for the brain. The software was adjusted to accommodate a 50 µm (scale bar) distance. The measurements of the areas mentioned were collected using the necessary instruments to determine the average distances (in µm2) of the respective components.

Statistical analysis

In this study, a One-Way ANOVA was performed to compare the means across multiple treatment groups. The mean ± standard error is used to present the results, with analyses conducted using GraphPad Prism 8 and SigmaPlot 12.0 software. Dunnett's test was applied for post-hoc comparisons to identify significant differences between treatment groups and a control group. This approach minimizes Type I errors while assessing multiple comparisons. Statistical significance was determined at a significance level of $P < 0.05$.

RESULTS AND DISCUSSION

Characterization undoped and Sn-doped ZnS NPs

UV-vis analysis

In the UV-Vis spectrum (Figure 1) of ZnS nanoparticles, the maximum absorption peak was observed at 303 nm. This peak signifies the wavelength at which the material absorbs light to the greatest extent. The absorption at 303 nm indicates that undoped ZnS NPs absorb light in the ultraviolet (UV) part of the spectrum. This absorption behavior results from transitions that occur within the crystal structure of ZnS. On the other hand, when we introduced Sn as a dopant into ZnS and examined its UV-Vis spectrum (Figure 1), we noticed a different absorption pattern. In this case, the maximum absorbance peak occurred at a wavelength precisely at 323 nm. The shift from 303 nm in ZnS to 323 nm in Sn-doped ZnS suggests that the presence of tin (Sn) dopants has altered the

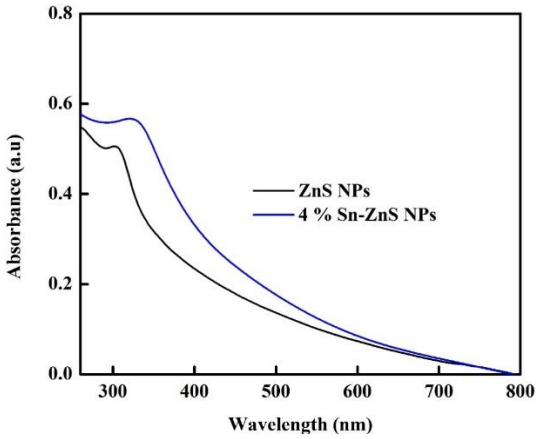

Fig. 1. UV-Vis spectra of undoped and Sn-doped ZnS NPs.

structure of ZnS, leading to changes in its optical properties. This shift can be explained by tin atoms incorporating into the ZnS crystal lattice and introducing energy levels that modify its band structure and consequently affect its absorption characteristics.

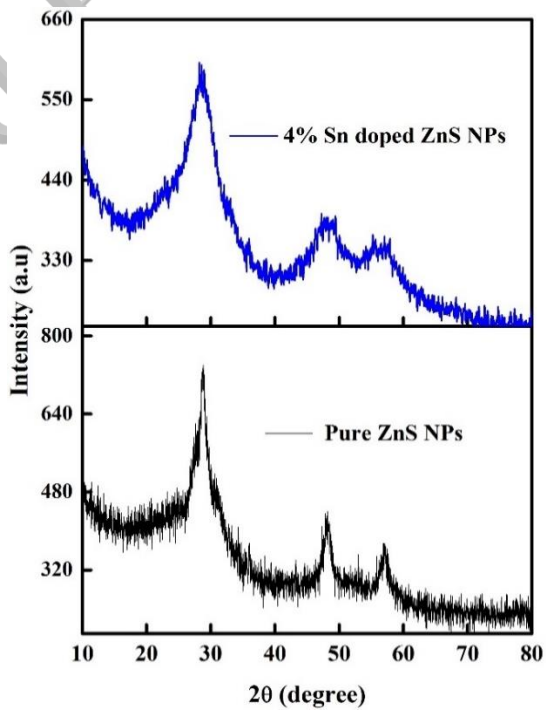

Fig. 2. XRD pattern of pure ZnS and Sn-doped ZnS nanoparticles.

XRD analysis

The XRD pattern of pure ZnS nanoparticles shows distinct diffraction peaks at 2 theta values of 28.78°, 47.86°, and 56.89°, corresponding to the crystallographic planes (111), (220), and (311), respectively, shown in Figure 2. The purity of the synthesized ZnS NPs is confirmed by these peaks,

which exhibit high conformance to the cubic zinc-blende structure (JCPDS No. 05-0566) [27]. The strong and well-defined peaks show that the nanoparticles have a high level of crystallinity. The XRD peaks of Sn-doped ZnS NPs and pure ZnS shows some peak broadening, indicating a reduction in particle size. According to an examination of the Debye-Scherrer equation, the average crystallite size is in the nanometer range, which is suggestive of the creation of nanoparticles [28, 29]. The average crystalline diameters of pure ZnS nanoparticles are 19.89 nm, while Sn-doped ZnS NPs are 16.54 nm.

Band gap calculation

Tauc's plot method was used to calculate the band gap energy of semiconductor materials using UV-Vis absorption spectra, as shown in Figure 3. The absorption coefficient (α) is calculated from absorption measurements at various wavelengths in the UV-Vis spectrum using this method. Then, for each data point, $(\alpha h\nu)^2$ was calculated, where α is the absorption coefficient, h is Planck's constant, and ν is the frequency of the incident photon. On a graph, these estimated values are shown against the respective photon energies (hυ) [30, 31]. For undoped ZnS nanoparticles, a band gap value of 3.50 eV is provided. The identical Tauc plot approach was used for Sn-doped ZnS NPs, where the specified band gap value is 3.10 eV.

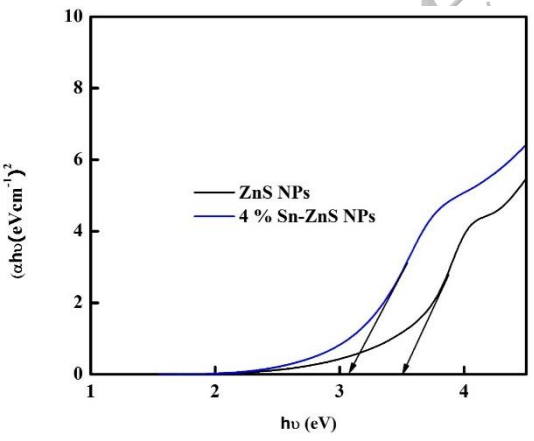

Fig. 3. Tauc's plots of undoped and Sn-doped ZnS NPs.

FTIR analysis

The FTIR provides essential details about the vibrational and structural properties of materials. As shown in Figure 4, the FTIR spectra of undoped and Sn-doped ZnS. The stretching vibrations, likely caused by hydrogen-bonded hydroxyl (OH) groups or the O-H stretching vibration of water molecules absorbed on the material's surface, are responsible

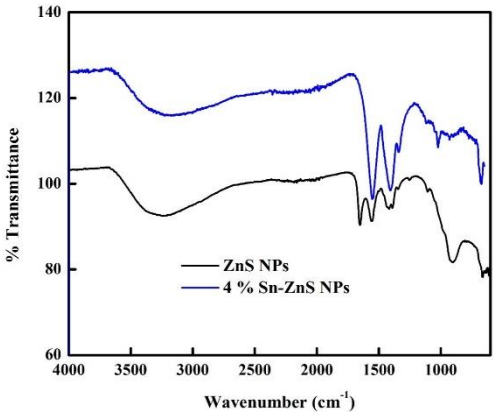

Fig. 4. FTIR spectra of both undoped and Sn-doped ZnS NPs.

for the band at 3270 cm^{-1}. There is an absorption at 1653 cm^{-1} that is suggestive of the bending or stretching vibrations associated with the Zn-S bond, which is a distinguishing property of the ZnS crystal lattice. Another band at 1554 cm^{-1} is most likely an extra Zn-S bond vibrational mode, probably a combination of bending and stretching vibrations. The band at 1384 cm^{-1} could represent lattice vibrations or other molecular vibrations inside the ZnS crystal structure. Additionally, the absorption at 901 cm^{-1} could be attributable to impurities or defects inside the undoped ZnS crystal lattice, whilst the band at 653 cm^{-1} could indicate additional lattice or molecular vibrations within the material. Some of these absorption bands changed from their original positions after tin (Sn) dopants were introduced into the ZnS lattice, suggesting changes in vibrational modes and bonding caused by the doping process. These shifts in the FTIR spectra of Sn-doped ZnS are caused by the incorporation of Sn atoms into the crystal structure, and they provide valuable insights into the structural and chemical changes caused by the doping, which can have significant implications for the material's properties and applications [27, 32].

SEM analysis

Figure 5a shows SEM images taken at a magnification scale of 100 nm, we can observe distinct differences between undoped and Sn-doped ZnS NPs. Undoped ZnS has unequal spherical morphologies with obvious aggregation, producing particle blocks or clusters. Sn-doped ZnS, on the other hand, has a more equal distribution of spherical nanoparticles throughout the sample, with a noticeable absence of large particle clusters. This morphological difference shows that adding tin (Sn) as a dopant has a dispersing impact on the ZnS nanoparticles, avoiding agglomeration and resulting in a more homogeneously dispersed structure are shown in Figure 5.

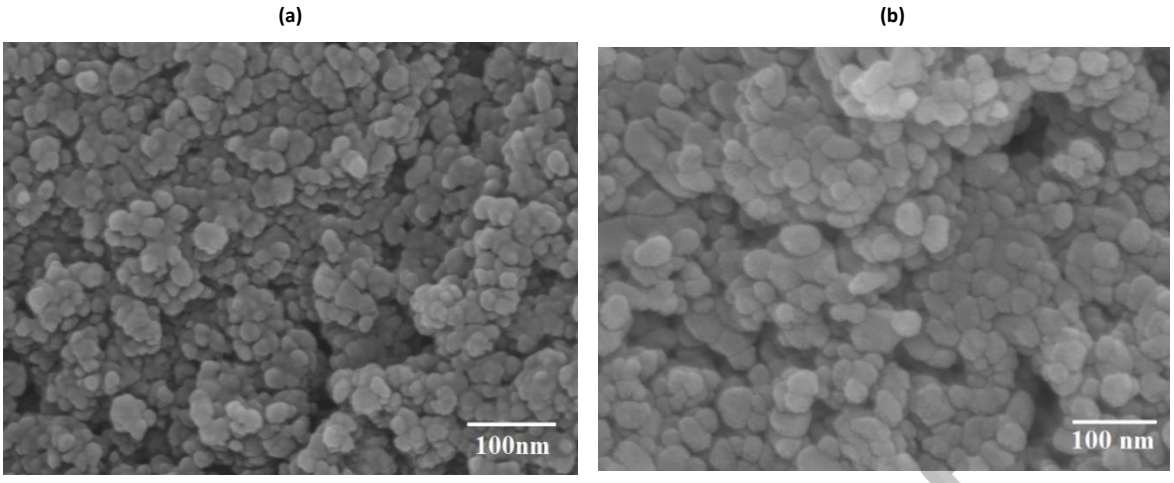

Fig. 5. SEM images of (a) undoped ZnS and (b) Sn-doped ZnS NPs.

EDX analysis

Energy Dispersive X-ray Spectroscopy (EDX) analysis confirmed that both doped and undoped nanoparticles contained their constituent elements in the expected proportions (Figure 6 (a) & (b)). The elemental composition analysis in both cases shows the presence of zinc (Zn), tin (Sn), and sulfur (S), and in the expected quantities. This confirms the precision and consistency of the sample preparation and analysis processes. The EDX pattern validates the compositional integrity of both nanoparticles, providing vital insight into the sample quality and consistency.

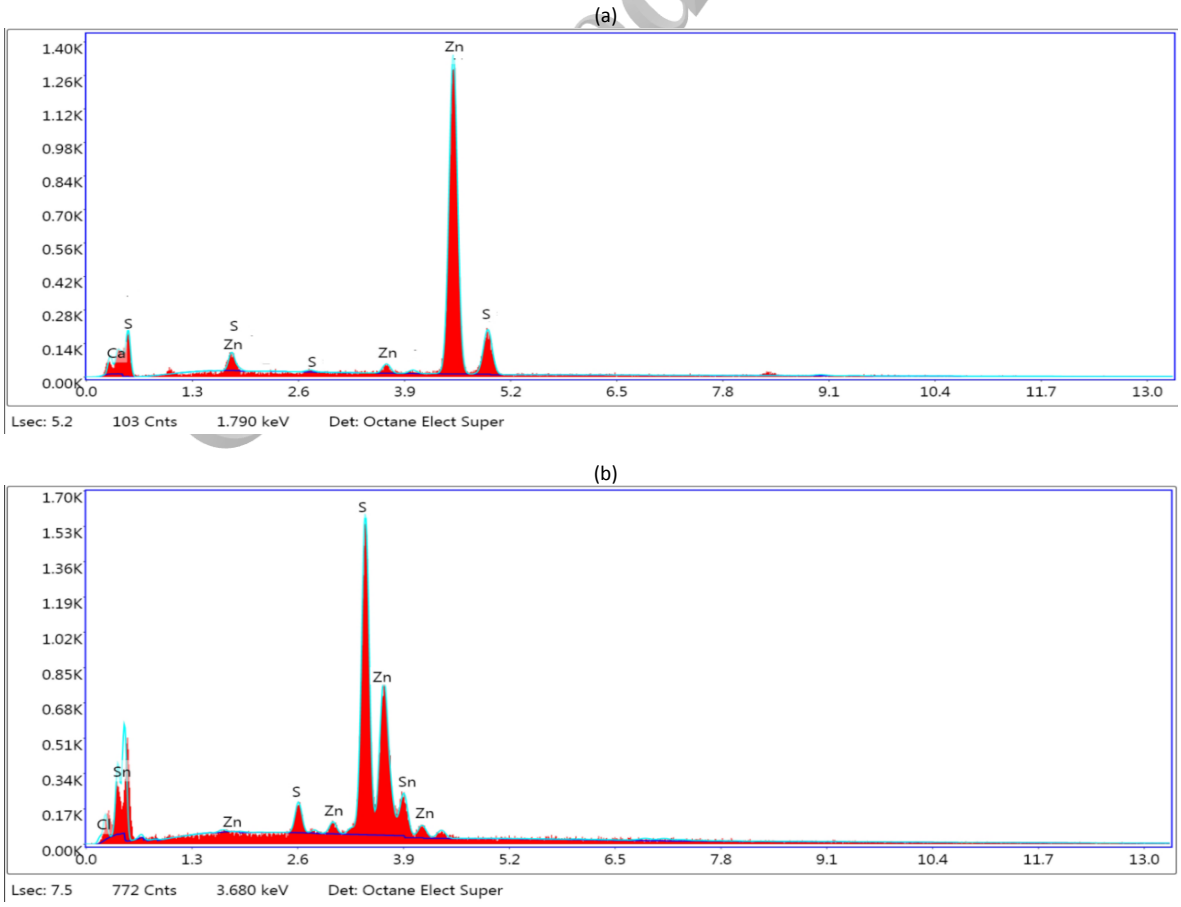

Fig. 6. EDX spectra of (a) undoped ZnS and (b) Sn-doped ZnS NPs.

Table 1. Male albino mice were intraperitoneally supplied with either saline solution or 5 mg/Kg body weight of ZnS-doped ZnS and Sn-doped ZnS for 14 days, and the various investigated organ mass index (OMI) values of the liver, kidney, and brain were compared between the treatment and control groups. The mean ± standard error is used for all values. The results of the two-sample One-Way ANOVA (Dennett's test) calculated for each parameter are shown by the P-values.

Groups	Liver	Kidney	Brain
Control	2.07 ±0.25	0.50 ± 0.03	0.45 ± 0.09
ZnS	2.08 ± 0.29	0.46 ± 0.02	0.49 ± 0.02
Sn/ZnS 4%	2.13 ± 0.19	0.50 ± 0.02	0.50 ± 0.02

Effect of undoped and Sn-doped ZnS nanoparticles on organ weight

The current study shows (Table 1) that pure ZnS and Sn-doped ZnS NPs have induced no clinical or behavioral changes in mice, while a non-significant difference in organ weight is observed. This serves as an effective benchmark for the qualitative assessment of the nanoparticles, indicating their potential to improve therapeutic ability, which aligns with previous literature [33]. The organ mass index (OMI) of the control group brain is 0.45 ± 0.09, while the ZnS and Sn-doped ZnS treated groups show slight fluctuations to 0.49 ± 0.02 and 0.50 ± 0.02, respectively (Table 1). The OMI of the liver is 2.07 ± 0.25 in the control group, followed by 2.08 ± 0.29 in the ZnS group and 2.13 ± 0.19 in the Sn-doped ZnS group. In the kidney, the OMI is 0.50 ± 0.03 in the control group, slightly reduced to 0.46 ± 0.02 in the ZnS group, and then reversed to 0.50 ± 0.02 in the Sn-doped ZnS group.

ZnS and Sn-doped ZnS nanoparticles on oxidative stress markers

Reactive oxygen species assay (ROS)

Oxidative stress is caused by zinc deficiency, and zinc supplementation has been shown to minimize oxidative damage in a variety of cells and tissues [34]. The ROS assay is performed to check the oxidative level in the brain, kidney, and liver. The ROS concentration in the Sn-doped ZnS-treated group shows a highly significant difference (0.001) in all organs (brain, kidney, and liver) as compared to the control, as detailed in Tables 2, 3, and 4, respectively. A noteworthy difference ($p<0.001$) in ZnS-treated group's kidney was found, while in the brain ($p<0.01$) and liver ($p<0.05$), significant differences were observed as compared to the control group.

Thiobarbituric acid reactive substance assay

Membrane lipid peroxidation results from oxidative stress, and measuring malondialdehyde (MDA) is a common way to detect oxidative stress [35]. MDA exhibits a pronounced binding preference towards thiol and amino functional groups in nucleic acids, peptides, and enzymes, consequently exerting potent cytotoxic effects on cellular systems [36]. Tbars concentration in the liver and brain is considerably ($p<0.001$) reduced in mice exposed to the Sn-doped ZnS NPs, as shown in Tables 4 and 2, respectively, while in the kidney, it was reduced ($p < 0.01$), as shown in Table 3. Tbars concentration in the ZnS-treated group ($p<0.001$) was reduced in the brain, while in the kidney and liver is ($p<0.05$).

Table 2. In comparison of antioxidant parameters of the brain between the control and treatment group, male albino mice were given intraperitoneally supplements of 5 mg/kg body weight of ZnS and Sn-doped ZnS or saline solution over 14 days. Mean ± standard error of the mean is the format used for all values. The results of the two-sample One-Way ANOVA (Dennett's test) are computed for each parameter and are shown by the *P*-values.

Parameters	Control	ZnS	Sn/ZnS 4%
ROS	18.59 ± 0.33	15.78 ± 0.29**	13.79 ± 0.41***
TBARS	16.30 ± 0.39	13.35 ± 0.10***	12.77 ±0.07***
SOD	12.33 ±1.45	19.16 ±1.22*	25.98 ± 057***
POD	16.01 ± 0.52	19.81 ± 0.37*	22.33 ± 1.35***
CAT	9.18 ± 0.57	11.37 ± 0.43*	16.01 ± 0.52***
GSH	15.78 ± 0.29	20.50 ± 0.66**	21.18 ± 0.688**
PE	9.06 ± 0.33	13.58 ± 0.30*	16.23 ± 1.86**

Table 3. For 14 days, male albino mice were given intraperitoneally supplementation of zinc and Sn-doped ZnS (5 mg/Kg body weight) or saline solution. This allowed for a comparison of several examined antioxidant parameters of the kidney between the treatment groups and the control. The mean ± standard error of the mean is displayed for each and every value.*P*-values display the results of the Dennis test (two-sample One-Way ANOVA), which were calculated for each parameter.

Parameters	Control	ZnS	Sn/ZnS 4%
ROS	18.96 ± 0.32	15.88 ± 032***	12.85 ± 032***
TBARS	16.56 ± 120	11.87 ± 088*	8.85 ± 0.66**
SOD	11.45 ±0.57	15.56 ±0.57*	18.69 ± 1.15***
POD	13.99 ± 0.09	20.18 ± 084**	25.47 ± 1.22***
CAT	7.13 ± 0.009	8.56 ± 033*	10.58 ± 034***
GSH	25.93 ± 1.20	31.75 ± 0.87*	36.07 ± 1.85**
PE	114.17 ± 1.72	121.21 ± 1.53*	122.61 ± 10.88*

Table 4. Male albino mice were given intraperitoneally supplements of either saline solution or 5 mg/kg body weight of ZnS and Sn-doped ZnS for 14 days. The aim was to compare the various investigated antioxidant parameters of the liver between the control and treatment groups. The format for all values is mean ± standard error. The results of the two-sample One-Way ANOVA (Dennett's test) are computed for each parameter and are shown by the *P*-values.

Parameters	Control	ZnS	Sn/ZnS 4%
ROS	12.47 ± 0.88	9.85 ± 0.34*	6.90 ± 0.33***
TBARS	25.20 ±0.57	21.59 ± 0.89*	17.99 ± 0.65***
SOD	12.15 ± 0.57	14.52 ± 0.30*	20.25 ± 0.56***
POD	16.85 ± 0.33	23.25 ± 1.15**	26.59 ± 1.19***
CAT	8.82 ± 0.33	12.53 ± 0.32***	16.24 ± 0.007***
GSH	18.24 ± 0.58	21.28 ± 0.58*	25.32 ± 0.57***
PE	80.80 ± 0.58	82.58 ± 0.33 *	83.53 ± 0.32**

ZnS and Sn-doped ZnS nanoparticles on antioxidant biomarkers

Superoxide dismutase (SOD)

The current study shows that ZnS and Sn-doped ZnS significantly increase superoxide dismutase (SOD) levels in the brains of treated mice. The SOD level in the ZnS-treated group is significantly increased ($p < 0.05$) in the brain, kidney, and liver compared to the control, as shown in Tables 2, 3, and 4, respectively. In the Sn-doped ZnS-treated group, SOD levels were highly significant ($p < 0.001$) compared to the control.

Peroxidase (POD)

Mice exposed to Sn-doped ZnS and ZnS will change their enzyme level in various organs. The present data revealed that Sn-doped ZnS significantly altered enzyme levels in the brain, kidney, and liver ($p < 0.001$), as shown in Tables 2, 3, and 4, respectively. In comparison to the control group, the brain of the ZnS-treated group revealed a significant difference ($p<0.05$), while the kidneys and liver revealed a significant difference ($p<0.01$).

Catalase (CAT)

One-way ANOVA of the treated groups (ZnS and Sn-doped ZnS) showed significant differences compared to the control. Catalase activity in the ZnS-treated group demonstrated a noteworthy difference ($p < 0.05$) in the brain and kidney, as shown in Tables 2 and 3, respectively, and a more pronounced difference ($p < 0.001$) In the liver significant difference is ($p < 0.001$) (Table 4). The Sn-doped ZnS-treated group also showed a highly noteworthy difference ($p < 0.001$) compared to the control group.

Reduced Glutathione (GSH)

One-way ANOVA of the treated groups (ZnS and Sn-doped ZnS) indicated a significant difference compared to the control. The Sn-doped ZnS-treated group shown a significant reduction in reduced glutathione in the liver ($p < 0.001$) (Table 4), while significant reductions were observed in the brain and kidney ($p < 0.01$), as indicated in Tables 2 and 3, respectively. The ZnS-treated group demonstrated a major difference ($p < 0.05$) in all organs except the brain, where the significance was ($p < 0.01$).

Protein estimation

The current study shows that mice treated with ZnS and Sn-doped ZnS significantly enhanced the protein level in all organs (brain, kidney, and liver). There was a significant difference ($p<0.05$) in the ZnS-treated group and a substantial difference ($p<0.01$) in the Sn-doped ZnS-treated group, with the exception of the kidney, which had a significance level of $p<0.05$. These findings are shown in Tables 2 and 4 for the brain, kidney, and liver, respectively.

Histopathology

Histology of the various organs, namely, brain, kidney, and liver, stained with hematoxylin and eosin (H&E), and subjected to analysis. No evident histopathological abnormalities or lesions associated with the treatment of nanoparticles (i.p) were observed in these animals. The brain exhibited no pathological abnormalities linked to the administration of nanoparticles. Necrosis, apoptosis, and mild vascular swelling were not detected in any of the histological samples examined, as presented in Figure 7. The liver of the treatment groups also had no histopathological changes; there was a normal sinusoidal space and hepatocyte distribution, as presented in Figure 7. The kidneys of the treated groups showed normal glomeruli, tubule, collecting ducts, and Bowman space as compared to the control, presented in Figure 7.

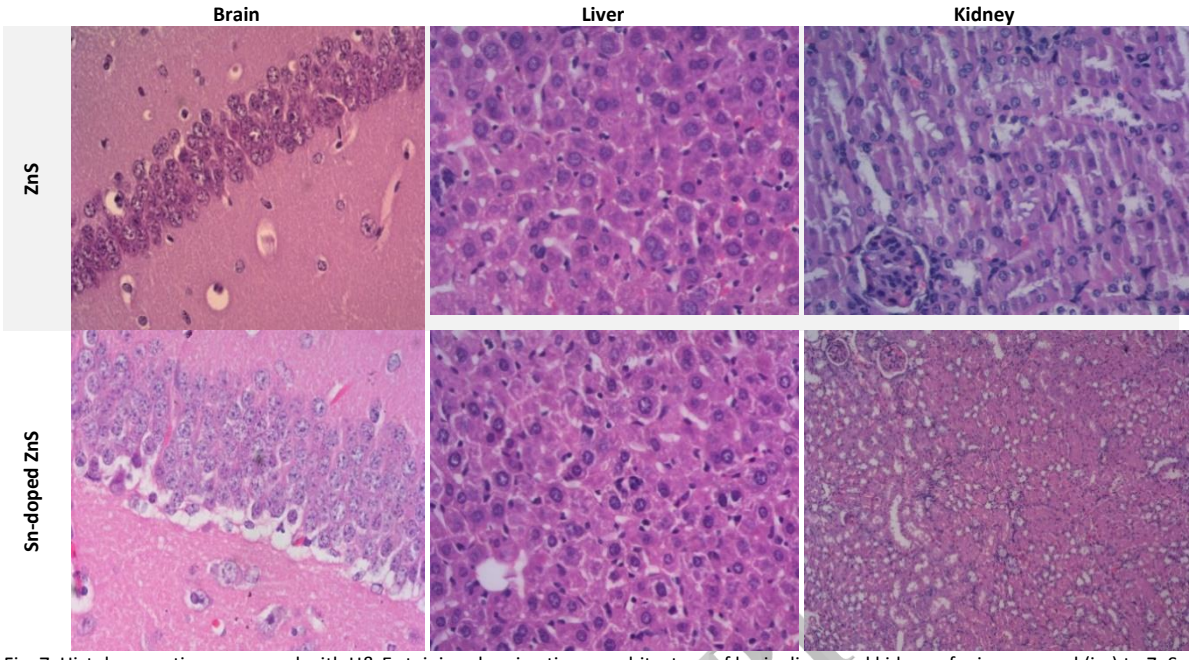

Fig. 7. Histology section processed with H& E staining showing tissue architecture of brain, liver, and kidney of mice exposed (i.p) to ZnS and Sn-doped ZnS. Magnification 40×. Scale bar: 50 µm.

Morphometry

Morphometry of the current studies revealed that treated and control group have no significant difference. ZnS and Sn-ZnS treated group showed a slight increase in the area of the liver (Hepatocyte and Nucleus area of hepatocyte), shown in Table 5, kidney: Glomerular area and renal corpuscular area as shown in Table 6, and in brain neuronal area shown in Table 7.

Table 5. Morphometry of mice liver following treatment with ZnS and Sn/ZnS. Values are mean ± S.E., n = 6.

Parameters	Control	ZnS	Sn doped ZnS
Hepatocyte area (µm²)	518.9±11.65	522.7±14.82[a]	525.0±15.64[a]
Nucleus area of Hepatocytes (µm²)	94.6, ±28.56	96.6, ±29.4[a]	98.3±30.0[a]

Common letter "a" = significantly different from control: *=p < 0.05, **= p < 0.01, ***= p < 0.001

Table 6. Morphometry of the mouse kidney following treatment with ZnS and Sn/ZnS. Values are mean ± S.E., n = 6.

Parameters	Control	ZnS	Sn doped ZnS
Glomerular area (µm²)	3689.54±396.75	3685.98±519.58[a]	3715.30±528.40[a]
Renal Corpuscular area (µm²)	4327.73±658	4380.71±678.53[a]	4478.52±678.00[a]

Common letter "a" = significantly different from control: *=p < 0.05, **= p < 0.01, ***= p < 0.001

Table 7. Morphometry of the mouse brain following treatment with ZnS and Sn/ZnS. Values are mean ± S.E., n = 6.

Parameters	Control	ZnS	Sn doped ZnS
Neuronal area (µm²)	3042.55±336.79	3080.54±348.72[a]	3140.98±352.50[a]

Common letter "a" = significantly different from control: *=p < 0.05, **= p < 0.01, ***= p < 0.001

Engineering and material science have been used in disease treatments, biosensors, advanced imaging, and drug and gene delivery [37]. Nanoparticles of small-sized metals lead to unique applications in biological, optical, and physicochemical science and may further be manipulated for anticipated applications [38]. For instance, gold nanoparticles are frequently used for biosensor labeling [39], silver nanoparticles in antimicrobial formulations [40], and magnetic nanoparticles have been investigated for in vitro or in vivo diagnostics [41]. Nanoparticles like tropical zinc oxide are used for diabetic foot ulcers and pressure ulcers to reduce the effects of bacteria [42]. Zinc is vital for humans because it functions as a cofactor in many transcription factors and enzymes that are important for growth, metabolism, and immunological function. Zinc is required for neurophysiology, which includes everything from cell development to cell proliferation, as well as antioxidant and immune system function. In severe neurological illnesses, it also plays a crucial pathophysiological function [43]. Additionally, zinc is

essential for reversing the toxic effects of inorganic compounds, which also change the histology in several organs, including the spleen, kidney, and liver [44].

ZnS nanoparticles are characterized by their attractive properties, which contribute to restricted areas of application, especially in pharmaceutics [45, 46]. ZnS nanoparticles play an essential role in the topical and systemic treatment of cancer [19]. ZnS possesses a semiconductor nanostructure that can generate singlet oxygen, hydroxyl radicals, and superoxide when photoexcited. After absorption of a wavelength equivalent to the band gap, charges could be transferred from the valence band to the empty conduction band, creating electron/hole pairs [47]. Still, excessive ROS generation can harm biological macromolecules and have negative consequences, including inflammation [48], fibrotic scarring [49], and senescence [50]. The present study was conducted to examine the therapeutic potential of undoped ZnS and Sn-doped ZnS nanoparticles on multiple organ systems, including the brain, kidney, and liver, with a focus on their prospective application in cancer treatment.

Organ mass index (OMI) was investigated after the dissection to identify the potential effects due to exposure to ZnS (undoped) and Sn-doped ZnS nanoparticles. The result showed that these nanoparticles did not cause any significant alteration in OMI-treated mice group samples (brain, kidney, and liver). Gross pathology analysis was performed to find the pathological or anatomical changes. Mice treated with ZnS and Sn-doped ZnS showed no observable clinical indications or behavioral changes [33]. The lack of evident organ-level pathological effects following their administration supports the idea that ZnS nanoparticles have a favorable safety profile and have no apparent pathological effects in the experimental paradigm, according to this research.

Reactive oxygen species serve as cell signaling molecules for regular biological functions, but their production may also affect numerous cellular organelles and processes, interrupting normal physiology [51]. Oxygen is present in large amounts and has a distinctive molecular structure. It quickly takes the free electrons produced by the cell's regular oxidative metabolism, which also produces the oxidant H_2O_2 and ROS such as the hydroxyl radical (HO•) and O_2•. Processes that cause electron transport uncoupling can increase ROS generation, with mitochondria being a main source [52]. ROS can induce direct harm to nucleic acids, proteins, and lipids via multiple pathways, resulting in cell death [53]. Our findings demonstrated that Sn-doped ZnS exhibits a significant ability to reverse the ROS level as compared to the control group, indicating that Sn-doped ZnS has potent properties. ZnS also showed protective effects, but least as compared to Sn-doped ZnS and the control group. These outcomes support the notion that the use of Sn-doped ZnS and ZnS can effectively mitigate ROS-induced damage, which is consistent with previous research highlighting the significance of sustaining the delicate balance between ROS generation and cellular antioxidant defenses [54]. Further study is needed to elucidate the specific mechanisms underlying the protective effects of these materials, which could lead to new applications in combating oxidative stress-related disorders.

MDA's chemical analysis began with its measurement as one of the TBARS to measure lipid peroxidation. It is difficult to determine TBARS in biological samples like serum and plasma in a reliable biological and analytical manner [55]. ZnS and Sn-doped ZnS also scavenge the effects of thiobarbituric acid reactive substances (TBARS) compared to the control group. TBARS are commonly used as markers of lipid peroxidation, which is a result of oxidative damage to lipids. Lipid peroxidation can lead to the formation of harmful by-products that can further damage cellular components. The findings of this study demonstrate that both ZnS and Sn-doped ZnS scavenge TBARS activity and mitigate lipid peroxidation and subsequent oxidative damage.

An extensive endogenous antioxidant defense system, which comprises endogenous antioxidant enzymes such as POD, CAT, SOD, GSH, and proteins, meticulously maintains cellular redox equilibrium. The human antioxidant defense is complex since it must minimize ROS levels while enabling ROS to play vital functions in cell signaling and redox control [56]. The mitochondrial respiratory chain generates the majority of physiological ROS, which is either transformed to hydrogen peroxide (H_2O_2) by spontaneous dismutation or catalyzed by SOD [57-59]. The current study outcomes revealed that Sn-doped ZnS and ZnS nanoparticles play an antioxidant role to enhance the level of SOD and CAT to reduce the level of ROS, as shown in Figure 8. In the free radical mechanism at 7.4 pH, superoxide ($\bullet O2^{-}$) is formed from O2 via the hydroperoxyl radical, whereas hydrogen peroxide (H_2O_2) is produced via mitochondrial respiratory by-products and NADPH oxidase. Superoxide dismutase (SOD) reduced Superoxide ($\bullet O2^{-}$) into (H_2O_2) via the Haber-Weiss reaction, which was subsequently converted into hydroxyl radicals ($\bullet OH^{-}$) and hydroxyl anions (•OH) and finally to water by catalase.

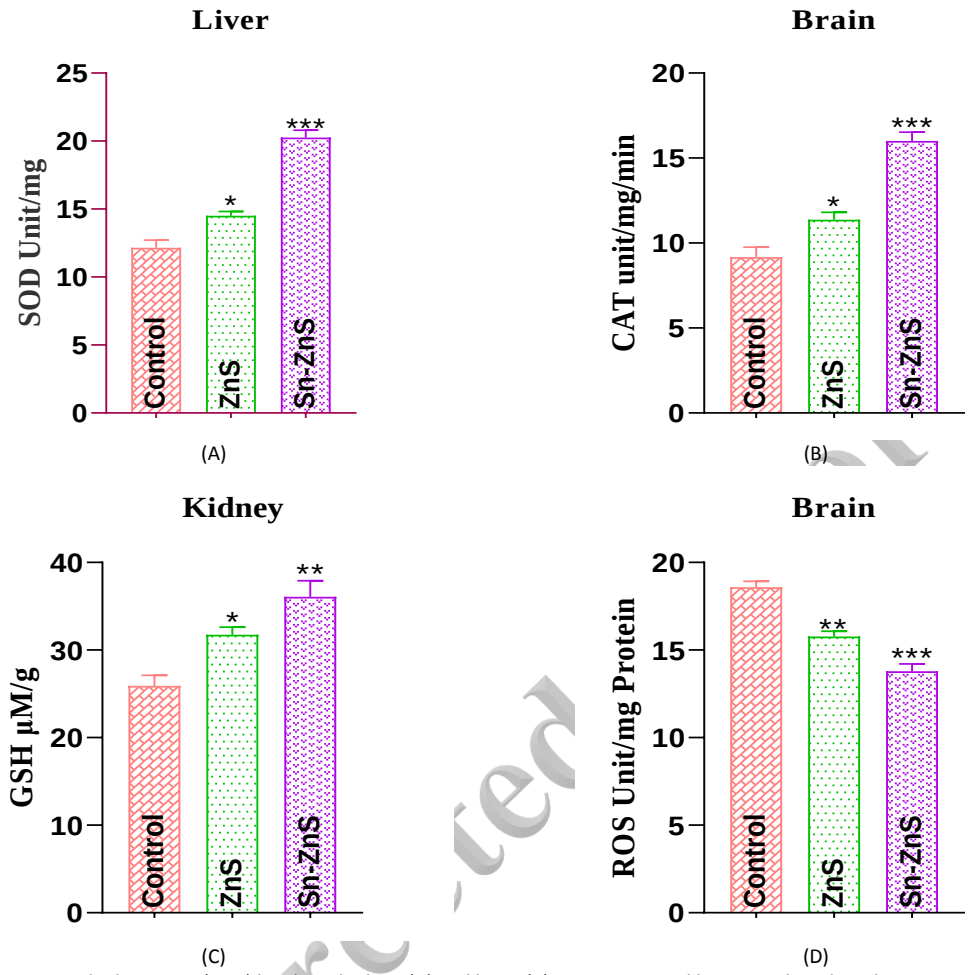

Fig. 8. Superoxide dismutase (SOD) levels in the liver (A) and brain (B) were recovered by ZnS and Sn-doped ZnS nanoparticles, and glutathione (GSH) in the kidney (C). Additionally, these nanoparticles reduced the level of ROS in the brain (D).

GSH is a thiol-containing compound and is central to various biological reactions [60]. GSH is also used as an inhibitor of tumor cells to prevent them from proliferating. ZnS and Sn-doped ZnS are also able to enhance the level of GSH to protect the cell from oxidative stress [61]. Zinc also inhibits oxidant enzyme and lipid peroxidation to protect the cell from oxidative damage [62]. It raises the level of activation of molecules and enzymes like antioxidant proteins, CAT, SOD, and GSH. Zinc catalyzes the dismutation of O_2^- into H_2O_2, a free radical scavenger, by forming MT, the cofactor for GSH [63, 64].

Histological examination of tissues was performed to further investigate toxicity. This approach can be used to assess tissue injury, lesions, or inflammation brought on by exposure to nanoparticles. Three organs, including the brain, kidney, and liver, were fixed, stained with Hematoxylin and Eosin, and examined. Overall, the administration of nanoparticles to these animals did not appear to cause any noticeable histological abnormalities or lesions (i.p). Figure 7 shows the histology results. The fact that there were no discernible changes in liver weight or observation suggests that the nanoparticles were removed. In the liver, there is no alteration in the histology. Hepatocytes are normal and help to maintain the homeostasis of the liver, such as carbohydrate, lipids, and protein metabolism, detoxification, and immune cell activation. Kidney histology shows that the normal Bowman capsule, and glomerulus tubule help to regulate the filtration of blood shown in Figure 7. The brain did not exhibit any pathological changes in response to nanoparticle treatment, as seen in Figure 7. These findings suggest that, at concentrations up to 5 mg/kg, ZnS and Sn-doped ZnS nanoparticles did not exhibit any harmful effects on cells [33].

CONCLUSION

This study confirms the in vivo protective efficiency of ZnS and Sn-doped ZnS NPs, with a particular emphasis on their potential in cancer

treatment. The study emphasizes the nanoparticles' favorable safety profile, which is demonstrated by the absence of organ-level adverse consequences. Furthermore, these nanoparticles have a noteworthy ability to alleviate the damage produced by ROS, highlighting their potential therapeutic utility. The research also reveals the antioxidant characteristics of these nanoparticles, highlighting their function in increasing levels of critical enzymes and substances, including SOD, CAT, and GSH. These findings point to a possible path for using ZnS and Sn-doped ZnS nanoparticles to combat oxidative stress and advance cancer therapy techniques. However, extensive investigations are required to clarify the underlying mechanisms of their biological effects, conduct in vitro studies, and explore their long-term safety profile.

AUTHORS CONTRIBUTION

Conceptualization, T.A., and F.A.J.; Methodology, T.A., F.A.J., N.U., H.S., H.A.; Software, T.A.; Validation, T.A., F.A.J., N.U.; Formal Analysis, T.A., and F.A.J.; Investigation, T.A., and F.A.J.; Resources, T.A., F.A.J., and H.S.; Data Curation, T.A.; Writing—Original Draft Preparation, T.A.; Writing—Review and Editing, T.A., and F.A.J.; Visualization, T.A.; Supervision, F.A.J.; Project Administration, F.A.J.; Funding Acquisition, T.A., and F.A.J. All authors have read and agreed to the published version of the manuscript.

ETHICAL APPROVAL

This research work was approved by the Ethical Committee of Quaid-i-Azam University, Islamabad (No.BEC-FBS-QAU2019-156).

FUNDING

Not applicable

AVAILABILITY OF DATA AND MATERIALS

The data will be available upon request to the corresponding author.

CONFLICTS OF INTEREST

The authors declare they have no conflict of interest.

REFERENCES

1. Haleem A, Javaid M, Singh RP, Rab S, Suman R. Applications of nanotechnology in medical field: a brief review. Global Health J. 2023; 7(2): 70-77.
2. Aththanayaka S, Thiripuranathar G, Ekanayake S. Emerging advances in biomimetic synthesis of nanocomposites and potential applications. Mater Today Sustain. 2022; 20: 100206.
3. Altammar KA. A review on nanoparticles: characteristics, synthesis, applications, and challenges. Front Microbiol. 2023; 14: 1155622.
4. Costa MI, Sarmento-Ribeiro AB, Gonçalves AC. Zinc: from biological functions to therapeutic potential. Int J Mol Sci. 2023; 24(5): 4822.
5. Ullah MI, Alameen AAM, Al-Oanzi ZH, Eltayeb LB, Atif M, Munir MU, Ejaz H. Biological role of zinc in liver cirrhosis: an updated review. Biomedicines. 2023; 11(4): 1094.
6. Chen B, Yu P, Chan WN, Xie F, Zhang Y, Liang L, et al. Cellular zinc metabolism and zinc signaling: from biological functions to diseases and therapeutic targets. Signal Transduct Target Ther. 2024; 9(1): 6.
7. Kloubert V, Rink L. Zinc as a micronutrient and its preventive role of oxidative damage in cells. Food Funct. 2015; 6(10): 3195-3204.
8. Narayan OP, Kumar P, Yadav B, Dua M, Johri AK. Sulfur nutrition and its role in plant growth and development. Plant Signal Behav. 2023; 18(1): 2030082.
9. Zhang X, Chen M, Ni X, Wang Y, Zheng X, Zhang H, et al. Metabolic reprogramming of sulfur in hepatocellular carcinoma and sulfane sulfur-triggered anti-cancer strategy. Front Pharmacol. 2020; 11: 571143.
10. Le Bars M, Legros S, Levard C, Chevassus-Rosset C, Montes M, Tella M, et al. Contrasted fate of zinc sulfide nanoparticles in soil revealed by a combination of X-ray absorption spectroscopy, diffusive gradient in thin films and isotope tracing. Environ Pollut. 2022; 292: 118414.
11. Ubaid KA, Zhang X, Sharma VK, Li L. Fate and risk of metal sulfide nanoparticles in the environment. Environ Chem Lett. 2020; 18(1): 97-111.
12. Durgadevi A, Dhayalini K, Nelson CC, Gunasingraj J, Hariharan P, Mohanraj S. Synthesis and characterization of ZnS nanoparticles. In: Hybrid and Advanced Technologies. CRC Press; 2025: 427-432.
13. Murugan S, Ashokkumar M, Nandhagopal M, Kumar KS. Dual-Doped Zinc Sulfide Nanosheets with Magnesium and Copper: Multifunctional Agents for Cancer, Microbial, Oxidative, and Hemolytic Defense. Microb Pathog. 2025; 107783.
14. Fernandez AC, Palanisamy S, Krishnan G, Priyadharsini N. Enhanced photoconductivity in SnO_2–ZnS nanocomposites: nano-structural, optical, and electrical investigations. J Nanopart Res. 2025; 27(7): 1–16.
15. Patel J, Jain B, Singh AK, Susan MABH, Jean-Paul L. Mn-doped ZnS quantum dots–an effective nanoscale sensor. Microchem J. 2020; 155: 104755.
16. Pareek A, Kumar D, Pareek A, Gupta MM. Advancing cancer therapy with quantum dots and other nanostructures: a review of drug delivery innovations, applications, and challenges. Cancers. 2025; 17(5): 878.
17. Li Z, Chu Z, Yang J, Qian H, Xu J, Chen B, et al. Immunogenic cell death augmented by manganese zinc sulfide nanoparticles for metastatic melanoma

immunotherapy. ACS Nano. 2022; 16(9): 15471-15483.
18. Hayes JD, Dinkova-Kostova AT, Tew KD. Oxidative stress in cancer. Cancer Cell. 2020; 38(2): 167-197.
19. Iqbal MJ, Kabeer A, Abbas Z, Siddiqui HA, Calina D, Sharifi-Rad J, Cho WC. Interplay of oxidative stress, cellular communication and signaling pathways in cancer. Cell Commun Signal. 2024; 22(1): 7.
20. Hussain MF, Naeem Ashiq M, Gulsher M, Akbar A, Iqbal F. Exposure to variable doses of nickel oxide nanoparticles disturbs serum biochemical parameters and oxidative stress biomarkers from vital organs of albino mice in a sex-specific manner. Biomarkers. 2020; 25(8): 719-724.
21. Ullah S, Akbar Jan F, Ullah N, Aziz T. Photocatalytic and therapeutic applications of the synthesized nickle oxide (NiO) nanoparticles. J Iran Chem Soc. 2023; 20(8): 2017-2029.
22. Ebrahim LK, Adel S, Hamza SA, Alsadany MA, Ali SM. Investigating the association between blood oxidative stress markers and dementia in Egyptian elderly women. Egypt J Neurol Psychiatry Neurosurg. 2024; 60(1): 73.
23. Murphy MP, Bayir H, Belousov V, Chang CJ, Davies KJ, Davies MJ, et al. Guidelines for measuring reactive oxygen species and oxidative damage in cells and in vivo. Nat Metab. 2022; 4(6): 651-662.
24. Hadwan MH, Hussein MJ, Mohammed RM, Hadwan AM, Saad Al-Kawaz H, Al-Obaidy SS, Al Talebi ZA. An improved method for measuring catalase activity in biological samples. Biol Methods Protocols. 2024; 9(1): bpae015.
25. Engelbrecht I, Horn S, Giesy JP, Pieters R. Determining superoxide dismutase content and catalase activity in mammalian cell lines. MethodsX. 2023; 11: 102395.
26. Sagar A, Sayyed RZ, Ramteke PW, Sharma S, Marraiki N, Elgorban AM, Syed A. ACC deaminase and antioxidant enzymes producing halophilic Enterobacter sp. PR14 promotes the growth of rice and millets under salinity stress. Physiol Mol Biol Plants. 2020; 26(9): 1847-1854.
27. Shah U, Jan FA, Ullah R, Wajidullah, Ullah N, Ahmad M. Photocatalytic degradation of acidic and basic dye by ZnS and tin-doped ZnS nanocatalysts. Iran J Sci. 2023; 47(3): 733-747.
28. Ramki K, RajaPriya A, Sakthivel P, Murugadoss G, Thangamuthu R, Rajesh Kumar M. Rapid degradation of organic dyes under sunlight using tin-doped ZnS nanoparticles. J Mater Sci Mater Electron. 2020; 31(11): 8750-8760.
29. Messalti AS, El-Ghozzi M, Zambon D, Mahiou R, Setifi Z. Investigating photoluminescence properties of Ca-doped ZnS nanoparticles prepared via hydrothermal method. J Luminesc. 2021; 238: 118227.
30. Boulkroune R, Sebais M, Messai Y, Bourzami R, Schmutz M, Blanck C, et al. Hydrothermal synthesis of strontium-doped ZnS nanoparticles: structural, electronic and photocatalytic investigations. Bull Mater Sci. 2019; 42(5): 223.
31. Dwivedi P, Chauhan P, Rawat RK. Effect of thermal treatment on synthesized Cu doped ZnS nanoparticles. Mater Today Proc. 2021; 44: 3138-3143.
32. Kumar S, Bhatti HS, Singh K, Gupta S, Sharma S, Kumar V, Choubey RK. Effect of glutathione capping on the antibacterial activity of tin doped ZnO nanoparticles. Physica Scripta. 2021; 96(12): 125807.
33. Reshma VG, Sabareeswaran A, Rajeev KS, Mohanan PV. In vitro and In vivo toxicity analysis of zinc selenium/zinc sulfide (ZnSe/ZnS) quantum dots. Food Chem Toxicol. 2020; 145: 111718.
34. Vali R, Shirvanian K, Farkhondeh T, Aschner M, Samini F, Samarghandian S. A review study on the effect of zinc on oxidative stress-related neurological disorders. J Trace Elem Med Biol. 2025; 88: 127618.
35. Roy Z, Bansal R, Siddiqui L, Chaudhary N. Understanding the role of free radicals and antioxidant enzymes in human diseases. Curr Pharm Biotechnol. 2023; 24(10): 1265-1276.
36. Pisoschi AM, Pop A, Iordache F, Stanca L, Predoi G, Serban AI. Oxidative stress mitigation by antioxidants-an overview on their chemistry and influences on health status. Eur J Med Chem. 2021; 209: 112891.
37. Sun L, Liu H, Ye Y, Lei Y, Islam R, Tan S, et al. Smart nanoparticles for cancer therapy. Signal Transduct Target Ther. 2023; 8(1): 418.
38. Wang S, Cheng K, Chen K, Xu C, Ma P, Dang G, et al. Nanoparticle-based medicines in clinical cancer therapy. Nano Today. 2022; 45: 101512.
39. Milan J, Niemczyk K, Kus-Liśkiewicz M. Treasure on the Earth—gold nanoparticles and their biomedical applications. Mater. 2022; 15(9): 3355.
40. Nie P, Zhao Y, Xu H. Synthesis, applications, toxicity and toxicity mechanisms of silver nanoparticles: A review. Ecotoxicol Environ Saf. 2023; 253: 114636.
41. Li X, Li W, Wang M, Liao Z. Magnetic nanoparticles for cancer theranostics: Advances and prospects. J Control Release. 2021; 335: 437-448.
42. Liu D, Liu L, Yao L, Peng X, Li Y, Jiang T, Kuang H. Synthesis of ZnO nanoparticles using radish root extract for effective wound dressing agents for diabetic foot ulcers in nursing care. J Drug Deliv Sci Technol. 2020; 55: 101364.
43. Choi S, Hong DK, Choi BY, Suh SW. Zinc in the brain: friend or foe?. Int J Mol Sci. 2020; 21(23): 8941.
44. Tizhe EV, Ibrahim NDG, Fatihu MY, Onyebuchi II, George BDJ, Ambali SF, Shallangwa JM. Influence of zinc supplementation on histopathological changes in the stomach, liver, kidney, brain, pancreas and spleen during subchronic exposure of Wistar rats to glyphosate. Comp Clin Pathol. 2014; 23(5): 1535-1543.
45. Chakrabarti A, Alessandri E. Syntheses, properties, and applications of ZnS-based nanomaterials. Appl Nano. 2024; 5(3): 116-142.
46. Yusuf A, Almotairy ARZ, Henidi H, Alshehri OY, Aldughaim MS. Nanoparticles as drug delivery systems: a review of the implication of nanoparticles' physicochemical properties on responses in biological systems. Polymers. 2023; 15(7): 1596.

47. Lu J, Guo Q, Chen J, Xie K, Guan X, Yang L, Wang G. Delicate design of ZnS@ In2S3 core–shell structures with modulated photocatalytic performance under simulated sunlight irradiation. ACS Omega. 2022; 8(1): 529-538.
48. Yu W, Tu Y, Long Z, Liu J, Kong D, Peng J, Hai C. Reactive oxygen species bridge the gap between chronic inflammation and tumor development. Oxid Med Cell Longev. 2022; 2022(1): 2606928.
49. Liu J, Han X, Zhang T, Tian K, Li Z, Luo F. Reactive oxygen species (ROS) scavenging biomaterials for anti-inflammatory diseases: from mechanism to therapy. J Hematol Oncol. 2023; 16(1): 116.
50. Guo J, Huang X, Dou L, Yan M, Shen T, Tang W, Li J. Aging and aging-related diseases: from molecular mechanisms to interventions and treatments. Signal Transduct Target Ther. 2022; 7(1): 391.
51. Auten RL, Davis JM. Oxygen toxicity and reactive oxygen species: the devil is in the details. Pediatr Res. 2009; 66(2): 121-127.
52. Polidori MC, Mecocci P. Modeling the dynamics of energy imbalance: The free radical theory of aging and frailty revisited. Free Radic Biol Med. 2022; 181: 235-240.
53. Juan CA, Pérez de la Lastra JM, Plou FJ, Pérez-Lebeña E. The chemistry of reactive oxygen species (ROS) revisited: outlining their role in biological macromolecules (DNA, lipids and proteins) and induced pathologies. Int J Mol Sci. 2021; 22(9): 4642.
54. Zhang B, Pan C, Feng C, Yan C, Yu Y, Chen Z, Wang X. Role of mitochondrial reactive oxygen species in homeostasis regulation. Redox Rep. 2022; 27(1): 45-52.
55. Mas-Bargues C, Escriva C, Dromant M, Borras C, Vina J. Lipid peroxidation as measured by chromatographic determination of malondialdehyde. Human plasma reference values in health and disease. Arch Biochem Biophys. 2021; 709: 108941.
56. Chaudhary P, Janmeda P, Docea AO, Yeskaliyeva B, Abdull Razis AF, Modu B, Sharifi-Rad J. Oxidative stress, free radicals and antioxidants: potential crosstalk in the pathophysiology of human diseases. Front Chem. 2023; 11: 1158198.
57. Napolitano G, Fasciolo G, Venditti P. Mitochondrial management of reactive oxygen species. Antioxidants. 2021; 10(11): 1824.
58. Kıran TR, Otlu O, Karabulut AB. Oxidative stress and antioxidants in health and disease. J Lab Med. 2023; 47(1): 1-11.
59. Konno T, Melo EP, Chambers JE, Avezov E. Intracellular sources of ROS/H2O2 in health and neurodegeneration: spotlight on endoplasmic reticulum. Cells. 2021; 10(2): 233.
60. Chai YC, Mieyal JJ. Glutathione and glutaredoxin—key players in cellular redox homeostasis and signaling. Antioxidants. 2023; 12(8): 1553.
61. Chun KS, Kim DH, Surh YJ. Role of reductive versus oxidative stress in tumor progression and anticancer drug resistance. Cells. 2021; 10(4): 758.
62. Niu B, Liao K, Zhou Y, Wen T, Quan G, Pan X, Wu C. Application of glutathione depletion in cancer therapy: Enhanced ROS-based therapy, ferroptosis, and chemotherapy. Biomaterials. 2021; 277: 121110.
63. Hübner C, Haase H. Interactions of zinc-and redox-signaling pathways. Redox Biol. 2021; 41: 101916.
64. Yang R, Roshani D, Gao B, Li P, Shang N. Metallothionein: a comprehensive review of its classification, structure, biological functions, and applications. Antioxidants. 2024; 13(7): 825.